RSC Advances

PAPER

View Article Online
View Journal | View Issue

Cite this: *RSC Adv.*, 2019, **9**, 13065

Optimum selective separation of Cu(II) using 3D ordered macroporous chitosan films with different pore sizes†

Yuzhe Zhang,[a] Tingting Bian,[a] Da Xia,[a] Dandan Wang,[a] Yi Zhang,[a]
Xudong Zheng ‡*[a] and Zhongyu Li ‡*[abc]

Received 29th January 2019
Accepted 6th April 2019

DOI: 10.1039/c9ra00773c

rsc.li/rsc-advances

Although bio-materials are widely used for the adsorption of heavy metal ions, they have low specific surface area, slow adsorption rates, and poor selectivity. To overcome these limitations, in this study, we report a 3D-ordered macroporous ion-imprinted chitosan film (3DOM-IICF); the 3DOM-IICF coupled with a colloidal crystal template and ion imprinting (IIP) technology has been used to absorb copper ions (Cu(II)) present in water. Moreover, polystyrene (PS) micro-spheres and copper templates were added to form a three-dimensional ordered macroporous structure and ion-imprinted sites, respectively. Finally, the film was formed by drying. Adsorption experiments showed the removal of Cu(II) from the 3DOM-IICF in an aqueous solution. The 3DOM-IICF exhibited good adsorption performance under neutral conditions of pH = 7.0, and the adsorption efficiency was high. The maximum adsorption capacity of the 3DOM-IICF was 261.31 mg g^{-1}. The adsorption processes were more consistent with the pseudo-second-order kinetic model and the Langmuir isotherm. The 3DOM-IICF exhibits superior selective adsorption of Cu(II). Moreover, the 3DOM-IICF could be regenerated multiple times, reused as an adsorbent and maintained high adsorption capacity. This kind of imprinted template method has important significance in the selective adsorption of pollutants in bio-materials and is worthy of in-depth research.

1. Introduction

Copper (Cu) is the main source of pollution from metal processing, machinery manufacturing, steel production and so on.[1] The metal toxicity of human beings increases after the intake of drinking water with high amount of Cu(II); moreover, Cu(II) combines with other toxins in water to generate more toxic organic substances;[2,3] to date, the methods used for the treatment of Cu(II) in an aqueous solution include chemical precipitation, redox reactions, solvent extraction, adsorption, and so on.[4] Among these methods, adsorption is considered as one of the fastest and most effective methods.[5] Activated carbon is the most common adsorbent used to remove heavy metals; however, activated carbon has many limitations, and it easily results in secondary pollution.[6] On the other hand, bacteria, yeast, and mold adsorbents have poor mechanical stability, weak selectivity for target adsorption, and slow adsorption rates. Therefore, the development of a highly efficient adsorbent is our primary goal.

Chitosan is a natural cationic polysaccharide; its biomass is huge, and it is the deacetylation product of chitin; thus, macromolecular chitosan has active hydroxyl and amino groups and strong chemical reaction ability.[7,8] Moreover, chitosan has unique physicochemical properties such as adsorption, film formation, fiber formation, moisture absorption and moisture retention. As a resource for utilization, chitosan has several advantages such as abundant raw materials, rapid regeneration, good environmental and bio-compatibility, and great significance for the treatment of water pollution, especially for the adsorption of heavy metal ions in water;[9] in addition, under certain conditions, chitosan undergoes hydrolysis, alkylation, acylation, carboxymethylation, sulfonation, nitration and other reactions; these reactions can produce a variety of chitosan derivatives with different properties, thereby expanding the scope of the application of chitosan. To increase the adsorption capacity of chitosan, several researchers have performed numerous modification studies using magnetic cross-linked chitosan materials and nanocomposite materials; Zhao's team has studied the synthesis of EDTA/DTDA cross-linked chitosan

---

[a] *School of Environmental and Safety Engineering, Changzhou University, Changzhou 213164, PR China. E-mail: zheng@cczu.edu.cn; zhongyuli@mail.tsinghua.edu.cn; Fax: +86-519-86330088; Tel: +86-519-86330088*

[b] *Jiangsu Key Laboratory of Advanced Catalytic Materials and Technology, School of Petrochemical Engineering, Changzhou University, Changzhou 213164, PR China*

[c] *Advanced Catalysis and Green Manufacturing Collaborative Innovation Center, Changzhou University, Changzhou 213164, PR China*

† Electronic supplementary information (ESI) available. See DOI: 10.1039/c9ra00773c

‡ Postal address: 417 Mingxing Building, Science and Education City, Wujin District, Changzhou, Jiangsu, China.

composite materials for the adsorption of heavy metal ions in an aqueous solution, and EDTA and DTDA have been used as cross-linking agents and functional groups; however, the performance of adsorbents under traditional cross-linking is not significant.[10] In many studies, composite nanomaterials are most popular among scholars. Aliabadi's team has studied chitosan@carboxy apatite composite nanomaterials.[11] Azzam's team has studied the effect of chitosan@clay composites and found that all these nanomaterials have large specific surface areas; however, the adsorption effect is indistinctive.[12] On this basis, Peng's group has prepared nanoporous magnetic cellulose@chitosan composite micro-sphere-adsorbed copper ions by the sol–gel transition method.[13] Although this method improves the defects of single magnetic materials and single nanomaterials, the magnetic micro-spheres adhere to the chitosan material; this leads to the loss of magnetic micro-spheres during adsorption. The research mentioned above has achieved certain achievements. However, the specific surface area of these materials is small, the mass transfer efficiency is low, and the selective adsorption capacity is weak or even absent. Therefore, the advantages of chitosan have not been exerted.

Forming a porous structure on chitosan seems to be a good way to solve the problem of low mass transfer efficiency. Hence, we coupled chitosan with colloidal crystal template PS micro-spheres. The advantages of PS micro-spheres with their controllable particle size, easy alignment and easy elution make these microspheres the best choice for templates.[14,15] In different porous materials, porous structures with a three-dimensional ordered arrangement have excellent specific surface area and exhibit excellent adsorption properties.[16]

Recently, many researchers have paid attention to the adsorption of Cu(II) in an aqueous solution by imprinted ions. Ion-imprinting is based on the fact that a polymer has specific ion-recognition sites that can be directly complementary to the target ions; the ion-imprinted polymers can be directly cross-linked by glutaraldehyde, cross-linking agents or functional groups, *etc.*[17,18] Chitosan has the advantages of abundant functional groups and easy cross linking, which make the method of imprinting easier in this case. To the best of our knowledge, most of the methods for imprinting ions result in the formation of micro-spheres or powders of chitosan.[19] However, the limited accessibility of the imprinted sites of these forms of chitosan greatly limits the adsorption selectivity and adsorption capacity as well as their application in industries. Among the many studies reported on the ion-imprinting technology, only few studies have been conducted on the adsorption behavior of heavy metal ions on imprinted films.[20,21]

A film structure is formed by the molecules spontaneously adsorbing at the solid–liquid interface *via* interaction between chemical bonds, thereby forming a thermodynamically stable self-assembled ordered film.[22–24] Compared with other methods, self-assembled film technology as a new material surface modification method has the advantages of wide molecular selection, simple and feasible preparation methods, mild preparation conditions and choice of various types of template materials; thus, it is expected to be widely used in aqueous systems.[25–28] In addition, the film-forming properties of chitosan contribute to the preparation of 3D ordered macroporous chitosan films. Since chitosan is a flexible material, we added TEOS to help stabilize the structure of chitosan and form an ordered structure. Therefore, we designed 3D ordered macroporous chitosan films with specific adsorption ability for Cu(II).

In this study, we prepared the 3DOM-IICF to adsorb Cu(II) from aqueous solutions. The 3D ordered macroporous structure of the material was characterized by scanning electron microscopy (SEM), transmission electron microscopy (TEM), Fourier transform infrared (FTIR) spectroscopy, thermogravimetric (TG) analysis and N_2 adsorption–desorption characterization. The adsorption properties of Cu(II) in an aqueous solution were studied and compared with those of the corresponding non-imprinted films. The effects of pH and temperature on the adsorption performance were systematically studied. In addition, we analyzed the effect of pore size on adsorption by changing the particle size of the PS microspheres.

2. Experimental

2.1 Preparation of materials

Chitosan (degree of deacetylation > 95%, viscosity 100–200 mPa s) was purchased from Sarn Chemical Technology Co., Ltd. (Shanghai, China). Ethyl orthosilicate (TEOS $(C_2H_5)_4SiO_4$), copper nitrate, glacial acetic acid, toluene, anhydrous ethanol and styrene were purchased from Sinopharm Group Chemical Reagent Co., Ltd. (Shanghai, China). Aladdin (Shanghai, China) provided glutaraldehyde (50%).

2.2 Instruments and equipment

The morphology of the surface samples was characterized by SEM (Hitachi S-4800) and TEM (SUPRA 55). The specific surface area of the samples was determined by the BET method (AUTOSORB-IQ2-MP). TG analysis was performed using a TG analyzer (Q600-TGA/DSC) under nitrogen conditions. The concentration of Cu(II) in the solution was determined using a flame atomic absorption spectrophotometer (AAS) (analytik jena, nova 300). The pH of the solution was measured using a digital pH meter (FE28-Standard, Mettler Toledo).

2.3 Preparation of materials

2.3.1 Synthesis of 200 nm polystyrene micro-spheres. The pretreatment of the purified styrene monomer involved mixing of the styrene monomer with an equal volume of an aqueous solution of 5 wt% NaOH; the oily substance in the upper layer was removed after standing the solution, and this procedure was repeated 3 times. The monomers were then further purified by distillation under reduced pressure.

At first, 10.0 g of purified styrene was mixed with 1.5 g of polyvinylpyrrolidone, and then, 90.0 g of double distilled water (DDW) was added. The solution was placed in a 250 mL flask and protected with nitrogen at 25 °C for 30 min. The mixture was then slowly heated to 70 °C. After this, 1.2 g of polystyrene and 10.0 g of distilled water were quickly added to the above-mentioned mixed solution to react for 24 h. The reacted solution was centrifuged, and polystyrene was rinsed with anhydrous ethanol followed by drying at 40 °C.

2.3.2 Synthesis of 500 nm polystyrene micro-spheres. At first, 9 mL of purified styrene, 0.5 mL of methyl methacrylate and 0.5 mL of acrylic acid were mixed well. Then, 0.11 g of ammonium persulfate and 0.486 g of ammonium carbonate were added to 60 mL of DDW. Both the abovementioned solutions were then placed in a 250 mL round-bottomed flask and mixed homogeneously. Under nitrogen protection, the reaction mixture was stirred at 70 °C for 16 h. The reacted solution was centrifuged, and polystyrene was rinsed with anhydrous ethanol followed by drying at 40 °C.

2.3.3 Synthesis of 1000 nm polystyrene micro-spheres. At first, 16.0 g of purified styrene was mixed with 0.12 g of polyvinylpyrrolidone and dissolved in 24 mL of DDW. Then, 0.3 g of ammonium persulfate was added. After this, the abovementioned solution was mixed with 200 mL of ethanol and poured into a 250 mL round-bottomed flask. After being protected with nitrogen at 25 °C for 30 min, the mixture was slowly heated to 70 °C for 16 h. The reacted solution was centrifuged, and polystyrene was rinsed with anhydrous ethanol followed by drying at 40 °C.

2.3.4 Synthesis of a 3D ordered macroporous imprinted chitosan film (3DOM-IICF). At first, 10.0 mg of $Cu(NO_3)_2$ was dissolved in a 20 mL of chitosan solution (40.0 mg of chitosan in a 50 mL of 1% acetic acid solution). Then, 200 mg of the prepared PS micro-spheres (200 nm, 500 nm and 1000 nm) was added to the abovementioned solution followed by the addition of 200 μL of tetraethyl orthosilicate. The mixed solution was then stirred at 60 °C for 2 h for sufficient hydrolysis. After the reaction was completed, the solution was poured into a Teflon mold and dried to form a film. The film scraped by soaked in 3% glutaraldehyde 30 min. Then, the prepared film was soaked in toluene for 30 min. By a Soxhlet extractor, the film soaked in the acetic acid solution for 2 weeks could wash away the printed metal ions. The 3D ordered macroporous non-imprinted chitosan film (3DOM-NIICF) was produced in the same way as the 3DOM-IICF without Cu(ɪɪ).

2.4 Adsorption experiment

The Cu(ɪɪ) stock solution was prepared from Cu nitrate and then diluted to the required concentration. The standard curve solution was prepared from a Cu standard solution.

The pH test was conducted by the following experiment: 10 mg of 3DOM-IICF and 3DOM-NIICF with 3 different particle sizes were immersed in Cu(ɪɪ) stock solutions (10 mL, 50 mg L^{-1}) with the pH values of 2.0, 4.0, 5.0, 6.0 and 7.0 and reacted for 24 h. The final concentration of Cu(ɪɪ) was determined by AAS. The pH adjustment of the Cu(ɪɪ) solution in the experiment was conducted using 0.1 M NaOH and 0.1 M HCl solutions. The adsorption capacity (Q_e) was calculated according to the following formula:

$$Q_e = \frac{V(C_0 - C_e)}{W} \tag{1}$$

C_0 (mg L^{-1}) is the initial concentration of the Cu(ɪɪ) solution, and C_e (mg L^{-1}) is the equilibrium concentration of the Cu(ɪɪ) solution. V is the volume of the solution, and W is the mass of the adsorbent.

The adsorption kinetics was studied by the following experiment: 10 mg of 3DOM-IICF and 3DOM-NIICF were immersed in a 10 mL Cu(ɪɪ) solution (50 mg L^{-1}, pH = 7.0) at 298 K. The experiment was conducted for 1–960 min. The residual concentration of Cu(ɪɪ) was determined by AAS.

The adsorption isotherm was obtained by the following experiment: 10 mg of 3DOM-IICF and 3DOM-NIICF with different particle sizes were immersed in Cu(ɪɪ) solutions at different concentrations (10 mL, pH = 7.0). The residual concentration was measured by AAS. The concentrations of the solutions were 10, 25, 50, 75, 100, 150, 200, 250 and 300 mg L^{-1}.

Competitive adsorption was studied by the following experiment. A mixed solution of Cu(ɪɪ), Cr(ɪɪɪ), Pb(ɪɪ) and Zn(ɪɪ) having the ion concentration of 50 mg L^{-1} was prepared. Then, 10 mg of 3DOM-IICF and 3DOM-NIICF were immersed in 10 mL of the abovementioned mixed solution at 298 K (pH = 7.0) and reacted for 24 h. Finally, the residual concentration was measured by AAS.

The adsorption thermodynamics was studied by the following experiment: 10 mg of 3DOM-IICF and 3DOM-NIICF were placed in a 10 mL Cu(ɪɪ) adsorption solution (pH = 7.0, 25, 50 and 150 mg L^{-1}) and reacted at 298, 308, 318 and 323 K for 24 h. Finally, the residual concentration was measured by AAS.

The regeneration experiment was conducted as follows: the Cu(ɪɪ) stock solution at the concentration of 50 mg L^{-1} was obtained, and the materials were eluted with an acetic acid solution (acetic acid : DDW = 1 : 9) until Cu(ɪɪ) was completely eluted. Then, the regenerated materials were adsorbed under the same conditions and passed through a flame atomic absorption spectrophotometer to measure the residual concentration. The test was repeated five times.

2.5 Characterization analysis

A series of characterizations of the successfully prepared 3DOM-IICF were performed. SEM and TEM were used to observe the morphological features as well as whether or not a 3D ordered macroporous structure was formed; moreover, FTIR was used to study the surface groups of the film. The surface structure characteristics of the film were characterized by nitrogen adsorption–desorption. TG analysis was conducted to investigate the thermal stability. The abovementioned five characterizations demonstrate that our material has a 3D ordered macroporous structure.

3. Results and discussion

3.1 Morphological analysis

We used SEM to observe the surface morphology of the template to verify if the PS colloidal crystal template was ordered. The SEM images obtained for three different particle sizes (200 nm, 500 nm and 1000 nm) of the PS colloidal crystal templates are

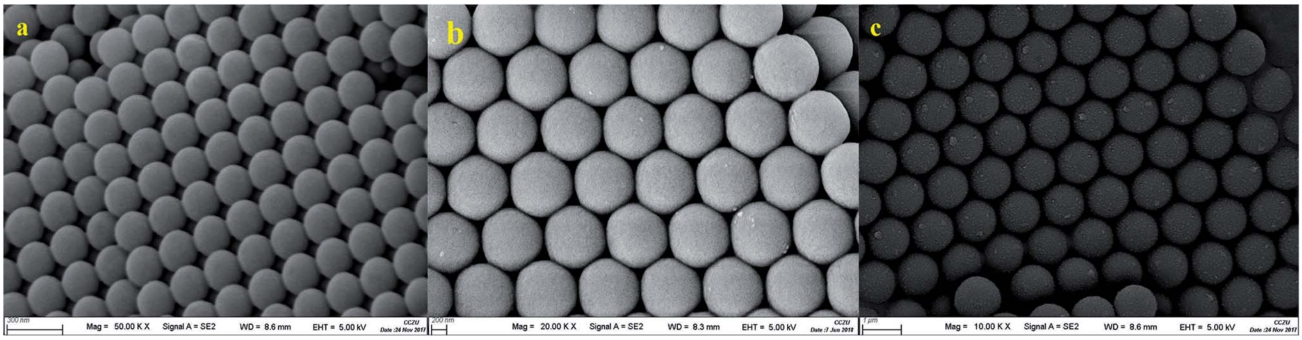

Fig. 1 SEM image of the PS microspheres ((a) shows the 200 nm PS microspheres, (b) shows the 500 nm PS microspheres, and (c) shows the 1000 nm PS microspheres).

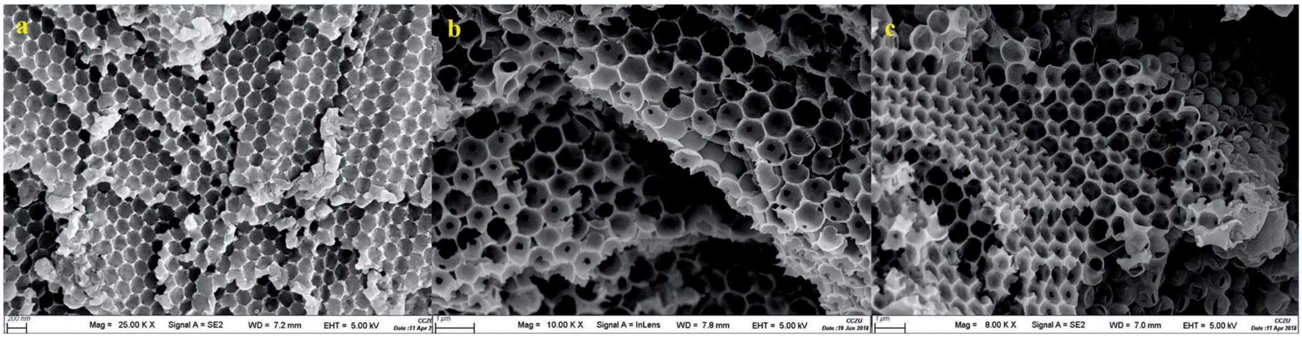

Fig. 2 SEM image of the 3DOM-IICF ((a) shows the 200 nm PS template; (b) shows the 500 nm PS template; and (c) shows the 1000 nm PS template).

shown in Fig. 1. It can be seen from Fig. 1 that the PS spheres with the three particle sizes are arranged in an ordered manner. It can be seen from the scale in the figure that the actual size of the three microspheres is not much different from the expected particle size, and the desired effect is achieved.

We further observed the surface morphology of the 3DOM-IICF using SEM to verify the formation of the 3D ordered macroporous structure. Fig. 2 shows an SEM image of a 3D ordered macroporous film made from PS templates with three particle sizes, which can be clearly seen from the surface topography of the material. Chitosan fills the gap in the template. The balls are eluted to form well-ordered holes, and the three-dimensional porous structure of the material can also be clearly seen in Fig. 2. The addition of TEOS in 3DOM-IICF maintains the stability of the material structure.

To verify the 3D ordered macroporous structure, we used TEM to characterize the internal structure of the material. Fig. 3 shows a TEM image of the 3DOM-IICF. We can clearly see the internal pore structure of the material in an orderly arrangement. The three-dimensional structure makes the images appear stacked one on top of another. As chitosan itself is soft and cannot tolerate high temperatures, this makes the material unable to withstand long-lasting strong voltage breakdown. The TEM image also demonstrates that the material has a 3D ordered pore structure.

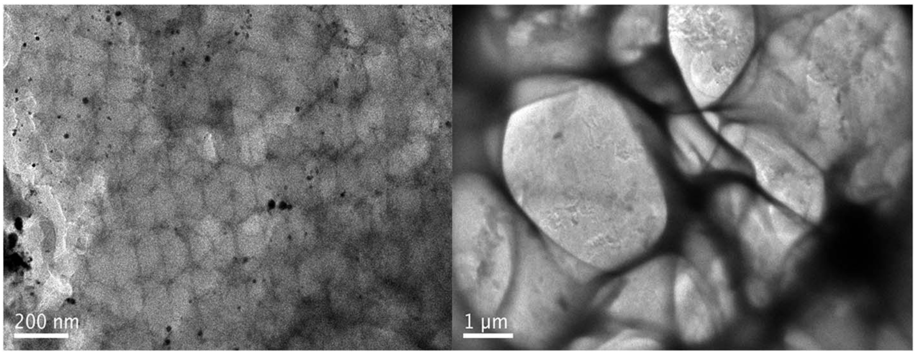

Fig. 3 TEM image of the 3DOM-IICF.

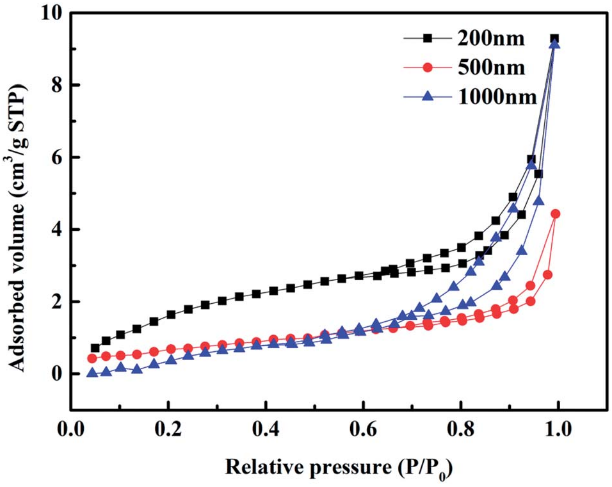

Fig. 4 N_2 adsorption–desorption isotherm plot of the 3DOM-IICF.

Table 1 Specific surface area of the 3DOM-IICF

Material	200 nm	500 nm	1000 nm
BET surface area (m^2 g^{-1})	7.6243	7.4522	4.9627

SEM and TEM were used to investigate the surface and interior of the material, and then, N_2 adsorption–desorption was used to further verify the pore structure of the 3DOM-IICF. Fig. 4 shows the N_2 adsorption–desorption isotherm plot of the 3DOM-IICF. It can be seen from the figure that the isotherm of the 3DOM-IICF belongs to type IV, and the material has a macroporous structure. The hysteresis loop of adsorption occurs at $P/P_0 = 0.7$–1.0 due to the capillary condensation of the porous adsorbent. After capillary condensation, the macroporous interactions may continue to result in multilayer adsorption; Table 1 shows the specific surface areas of particles with three particle sizes. The specific surface areas of the 200 nm, 500 nm and 1000 nm 3DOM-IICF are 7.6243, 7.4522 and 4.9627 m^2 g^{-1}, respectively. The larger the pore size of the material, the smaller the specific surface area. Due to the large pore size and the reduced number of pores, a small specific surface area was obtained.

3.2 FTIR spectroscopy

FTIR spectroscopy was used to analyze the functional groups on the surface of 3DOM-IICF. The FTIR spectrum of the film is shown in Fig. 5. The visible peaks of 3DOM-IICF and 3DOM-NIICF in the range of 4000–500 cm^{-1} are similar. The absorption peak at about 3448 cm^{-1} is attributed to the stretching vibration of –NH$_2$ and –OH. Moreover, the unique absorption peaks generated at about 3002 and 2852 cm^{-1} are caused by the stretching vibrations of –CH, –CH$_2$ and –CH$_3$. The absorption peak at about 1654 cm^{-1} is due to the bending vibration of –NH in –NH$_2$. The stretching vibration of C=O in the *N*-acetyl group resulted in a distinct absorption peak at about 1535 cm^{-1}. The absorption peak at about 1071 cm^{-1} is attributed to the stretching vibration at the C–O–C bridge. These absorption peaks indicate that chitosan has been successfully adhered to the PS micro-sphere gap and formed a proportion of pore structure.

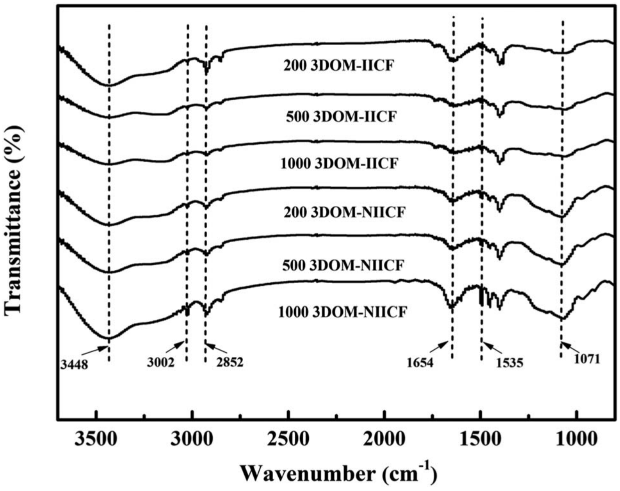

Fig. 5 The FTIR spectra of 3DOM-IICF and 3DOM-NIICF.

3.3 TG analysis

TG analysis of the 3DOM-IICF and 3DOM-NIICF was carried out under the protection of nitrogen. Fig. 6 shows a graph of the change in temperature from room temperature to 800 °C at the rate of 10 °C min^{-1} and the total weight as a function of temperature. The total weight loss of the six materials is between 65 and 72%. When the temperature was increased to 100 °C, the total weight loss was about 8%. This part of the lost weight was mainly due to the loss of residual water. Thus, it can be concluded that this material is a hydrophilic material. The loss of total weight at 0–400 °C is relatively gentle; this indicates that the material has excellent thermal stability. At 200 °C, the 3DOM-IICF began to decompose because the addition of TEOS increased the thermal stability of the material. Between 400 and 470 °C, the total weight loss reached about 40%, and the final weight loss was attributed to the loss of residual silicon material, which enhanced the thermal stability.

3.4 Adsorption experiment

3.4.1 Effect of pH. The pH value of the solution is one of the important factors affecting the adsorption capacity of the material. Since Cu(II) will form the Cu(OH)$_2$ precipitate under alkaline conditions, the pH value in the experiment was chosen 5 points between 2.0 and 7.0. It can be seen from Fig. 7 that the lowest adsorption capacity is obtained at pH = 2.0. The possible reason is that the acidic state of the solution leads to severe protonation of the amino group of chitosan; thus, Cu(II) cannot chelate with the amino group, and the adsorption capacity decreases. As the pH value increases, the degree of protonation decreases, and the amount of adsorption increases. This result is consistent with the measurement of the zeta potential

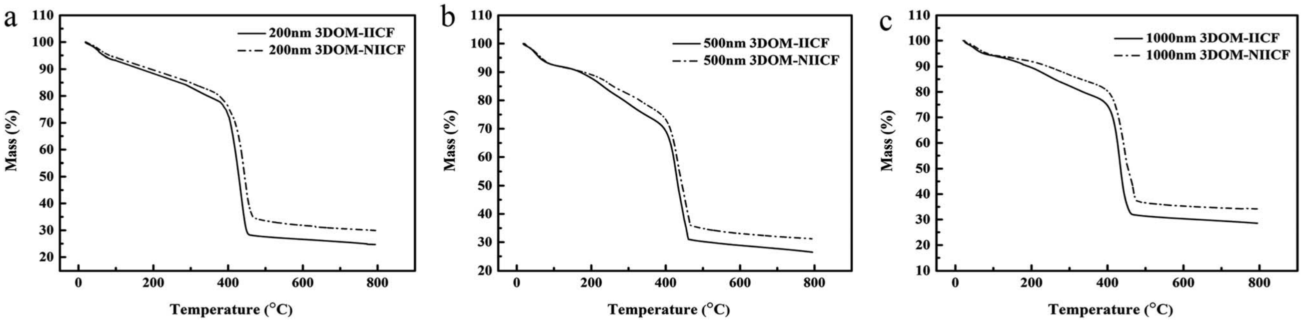

Fig. 6 Thermogravimetry data of 3DOM-IICF and 3DOM-NIICF.

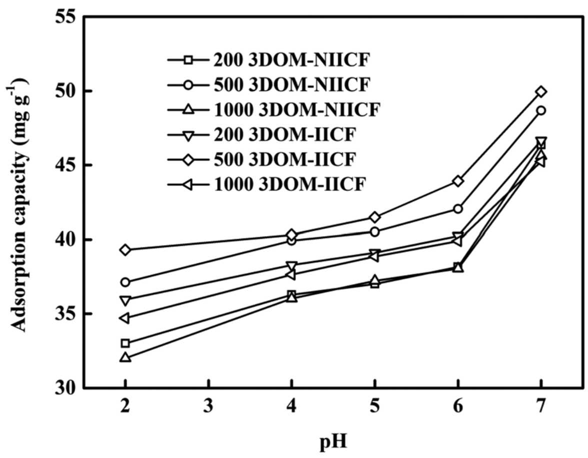

Fig. 7 Effect of pH on the adsorption of Cu(II) on 3DOM-IICF and 3DOM-NIICF.

(Fig. S1†). It can also be clearly seen from Fig. 7 that the adsorption capacity of the 3DOM-IICF is better than that of the 3DOM-NIICF. In the case of the 3DOM-IICF, the 500 nm pore-sized film has the best adsorption efficiency because it not only has higher specific surface area, but also increases the mass transfer efficiency due to the larger pore size; the second highest adsorption efficiency is of the 200 nm pore-sized film because its specific surface area is much larger than that of a 1000 nm pore-sized film; thus, the pH value has been adjusted to 7.0 for all subsequent experimental solutions of Cu(II) in this experiment.

3.4.2 Adsorption kinetics. Before fitting the adsorption data, the amount of Cu(II) adsorbed at time *t* was first calculated using the eqn (2):

$$Q_t = \frac{V(C_0 - C_t)}{W} \tag{2}$$

where Q_t (mg g^{-1}) refers to the amount of Cu(II) adsorbed at time t, C_0 (mg L^{-1}) refers to the concentration of the solution before adsorption, C_t (mg L^{-1}) refers to the equilibrium concentrations at time t, and V and W are the volume of the solution participating in the adsorption reaction and the mass of the adsorbent, respectively.

Adsorption kinetic data were fitted. The commonly used fitting models were pseudo-first-order kinetic model (PFOKM) and pseudo-second-order kinetic model (PSOKM). They were used to test the adsorption data. The fitting formulas of the PFOKM and PSOKM were

$$Q_t = Q_e - Q_e e^{-k_1 t} \tag{3}$$

$$Q_t = \frac{k_2 {Q_e}^2 t}{1 + k_2 Q_e t} \tag{4}$$

The initial adsorption rate h (mg g^{-1} min^{-1}) and the half-equilibration time $t_{1/2}$ (min) of the PSOKM were obtained according to the formulas (5) and (6), respectively:

$$h = k_2 {Q_e}^2 \tag{5}$$

$$t_{1/2} = \frac{1}{k_2 Q_e} \tag{6}$$

where Q_t (mg g^{-1}) represents the amount of Cu(II) adsorbed at time t, Q_e (mg g^{-1}) represents the adsorption amount at equilibrium, t (min) is the time, k_1 is the rate constant of PFOKM, and k_2 is the rate constant for PSOKM.

Fig. 8 shows a comparison between the adsorption kinetics of 3DOM-IICF and 3DOM-NIICF at 298 K, pH = 7.0 and 50 mg L^{-1} and a comparison for the three particle sizes. It can be clearly seen from Fig. 8 that the adsorption rate of the macroporous chitosan film is rapid, and the adsorption amount can reach approximately 30 mg g^{-1} in 0–100 min. After 200 min, the adsorption was slow, and it gradually reached adsorption equilibrium. From Fig. 8a and b, it can be seen that regardless of 3DOM-IICF or 3DOM-NIICF, the best adsorption capacity among the films with three different particle sizes was exhibited by the 500 nm pore-sized film, followed by the 200 nm and 1000 nm pore-sized films. A number of amino groups of the biosorbent chitosan resulted in fast adsorption efficiency. The 200 nm and 500 nm chitosan films have large specific surface area, which leads to high adsorption capacity. Among them, the 500 nm chitosan film has large pore size, resulting in highest adsorption capacity of the material in this experiment. It can be clearly seen that regardless of the pore sizes, the 3DOM-IICF has better adsorption performance than the 3DOM-NIICF. This material is more in line with PSOKM; this indicates that the

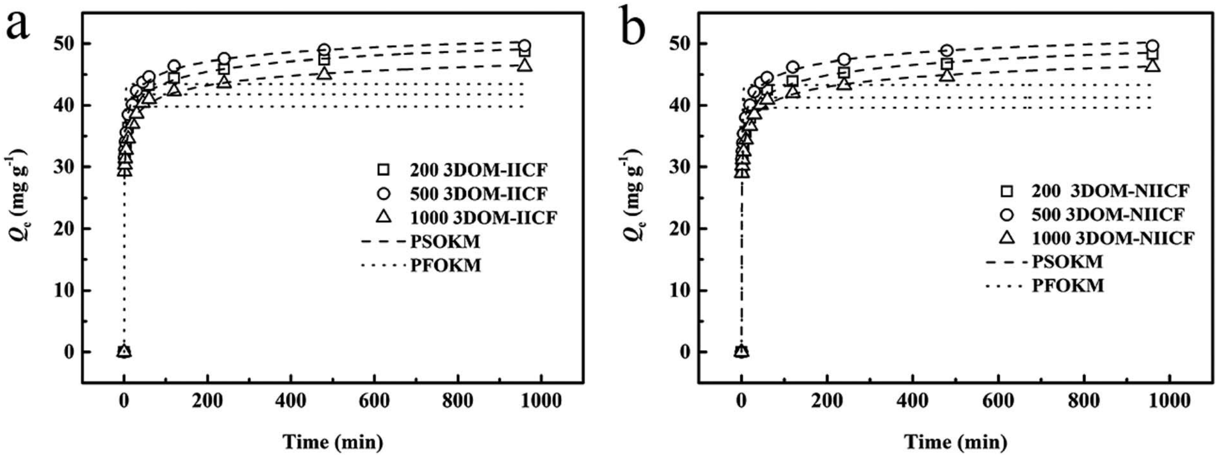

Fig. 8 Kinetic data and model of Cu(II) adsorption on 3D-MCF. (a) shows a comparison chart of 3DOM-IICF; (b) shows a comparison chart of 3DOM-NIICF.

Table 2 Kinetic constants for the PFOKM and PSOKM

		PFOKM			PSOKM				
Materials	$Q_{e,exp}$ (mg g^{-1})	$Q_{e,c}$ (mg g^{-1})	k_1 (min^{-1})	R^2	$Q_{e,c}$ (mg g^{-1})	$K_2 \times 10^{-2}$ (g mg^{-1} min^{-1})	h (mg g^{-1} min^{-1})	$t_{1/2}$ (min)	R^2
200 nm 3DOM-IICF	46.65	39.75	0.87	0.844	58.66	1.59	54.55	1.08	0.991
500 nm 3DOM-IICF	49.66	43.34	0.82	0.854	58.20	1.86	62.90	0.93	0.991
1000 nm 3DOM-IICF	46.31	39.61	0.87	0.847	57.48	1.67	55.31	1.04	0.990
200 nm 3DOM-NIICF	46.42	41.74	1.45	0.680	59.16	1.60	55.83	1.06	0.992
500 nm 3DOM-NIICF	49.63	43.47	0.84	0.856	58.24	1.89	64.06	0.91	0.991
1000 nm 3DOM-NIICF	46.23	39.83	0.87	0.847	57.37	1.70	56.09	1.02	0.990

adsorption method is more in line with chemical adsorption, and the correlation coefficients (R^2) between 3DOM-IICF and PSOKM are 0.991, 0.991 and 0.990 in the order of the pore sizes from small to large. The correlation coefficients (R^2) between 3DOM-NIICF and PSOKM are 0.992, 0.991, and 0.990. The relevant data of the dynamics fitting are shown in Table 2.

3.4.3 **Adsorption isotherms.** To investigate the adsorption capacities of 3DOM-IICF and 3DOM-NIICF at different concentrations, we conducted an adsorption isotherm experiment. The Langmuir and Freundlich isotherms were fitted to the adsorption data, and the equations for the Langmuir and Freundlich isotherms are as follows:

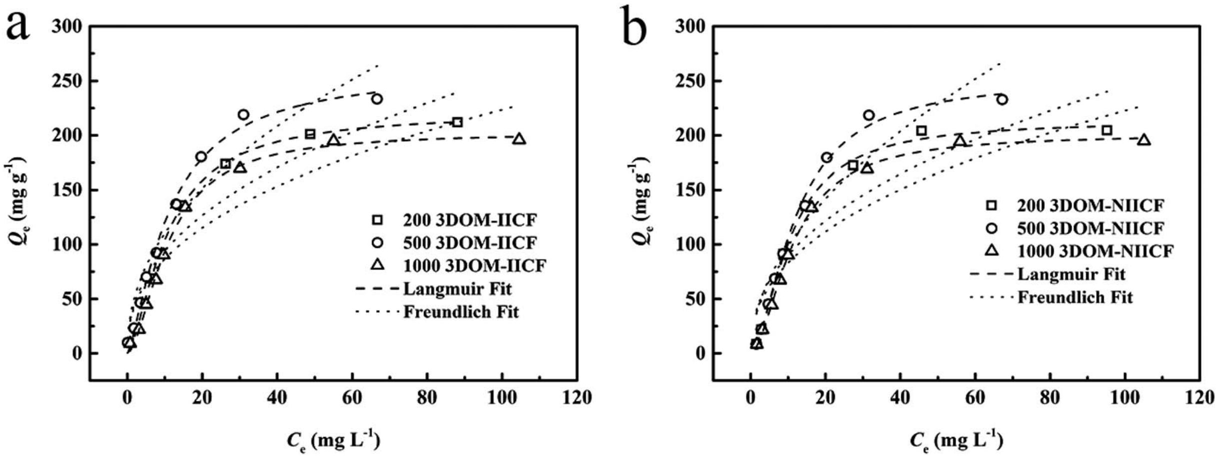

Fig. 9 Isotherm model fitting of 3D-MCF adsorbing Cu(II). (a) shows a comparison chart of 3DOM-IICF; (b) shows a comparison chart of 3DOM-NIICF.

Table 3 Adsorption equilibrium constants for the Langmuir and Freundlich isotherm equations

	Langmuir isotherm equation				Freundlich isotherm equation		
Sorbents	R^2	K_L (L mg^{-1})	Q_m (mg g^{-1})	R_L	R^2	K_F (mg g^{-1})	1/n
200 nm 3DOM-IICF	0.995	0.019	202.89	0.216	0.859	35.436	0.400
500 nm 3DOM-IICF	0.992	0.038	261.31	0.102	0.910	38.128	0.461
1000 nm 3DOM-IICF	0.996	0.017	203.01	0.228	0.855	33.518	0.412
200 nm 3DOM-NIICF	0.998	0.015	201.52	0.251	0.840	31.561	0.425
500 nm 3DOM-NIICF	0.995	0.016	252.23	0.209	0.871	29.642	0.523
1000 nm 3DOM-NIICF	0.998	0.014	201.29	0.266	0.842	30.886	0.429

Table 4 Thermodynamic parameters for the Cu(II) adsorption

Materials	ΔH (kJ mol^{-1})	ΔS (J mol^{-1})	T (K)	K^0	ΔG (kJ mol^{-1})	R^2
200 nm 3DOM-IICF	21.96	88.69	298	6.19	−4.52	0.993
			308	7.91	−5.30	
			318	10.55	−6.23	
			323	12.28	−6.74	
500 nm 3DOM-IICF	23.44	92.36	298	5.29	−0.09	0.995
			308	6.92	−0.13	
			318	9.40	−0.20	
			323	10.99	−0.25	
1000 nm 3DOM-IICF	22.86	89.79	298	4.88	−0.07	0.998
			308	6.42	−0.11	
			318	8.70	−0.170	
			323	9.90	−0.210	

$$Q_e = \frac{K_L Q_m C_e}{1 + K_L C_e} \tag{7}$$

$$Q_e = K_F {C_e}^{1/n} \tag{8}$$

where Q_m (mg g^{-1}) represents the maximum adsorption capacity, and K_L (L g^{-1}) and K_F (mg g^{-1}) represent the affinity constants of the Langmuir isotherm and the direction constant of the Freundlich isotherm, respectively. 1/n represents a heterogeneity factor. Using the separation factor R_L to analyze the advantages of adsorption, the formula for R_L was obtained as follows:

$$R_L = \frac{1}{1 + C_m K_L} \tag{9}$$

where C_m is the maximum initial value of Cu(II) concentration.

Fig. 9 shows a comparison between the adsorption isotherm fits of the six materials. It can be clearly seen from the figure that 3DOM-IICF (200 nm, 500 nm and 1000 nm) and 3DOM-NIICF (200 nm, 500 nm and 1000 nm) are more in line with the Langmuir isotherm. The isotherm shows that the adsorption method of the experimental material is monomolecular chemical adsorption.

The correlation coefficients (R^2) of 3DOM-IICF and 3DOM-NIICF with the Langmuir isotherms were 0.995, 0.992, 0.996, 0.998, 0.995 and 0.998 in the order of the pore sizes from small to large. With an increase in the concentration of the adsorbent solution, the adsorbent gradually reached adsorption saturation, and the maximum adsorption capacity of the 3DOM-IICF material was 261.31 mg g^{-1}. The other adsorption fitting data are shown in Table 3.

It can be seen from Table 3 that the R_L value of the 3DOM-IICF is smaller than that of 3DOM-NIICF, and the R_L values of the 3DOM-IICF are 0.216, 0.102 and 0.228, which indicate that 3DOM-IICF is more favorable for the adsorption of Cu(II). Herein, 500 nm 3DOM-IICF was the most favorable adsorbent.

3.4.4 Adsorption thermodynamics. To further verify the adsorption performance of the 3DOM-IICF, we studied the effect of temperature on the adsorption efficiency. The Gibbs free energy ΔG was used to predict the adsorption method and the adsorption feasibility. The formula for ΔG is as follows:

$$\Delta G = -RT \ln K^0 \tag{10}$$

where K^0 is a thermodynamic equilibrium constant. The values of the standard enthalpy ΔH and the entropy ΔS were calculated by the van't Hoff equation. The formula is as follows:

$$\ln K^0 = \frac{\Delta S}{R} - \frac{\Delta H}{RT} \tag{11}$$

where ΔH is the slope of the curve, ΔS is the intercept of the curve, and T (K) is the temperature. The results obtained by calculating the relevant data are shown in Table 4.

Fig. 10 shows the overall situation of the adsorption thermodynamics. With an increase in temperature, the adsorption capacity of 3DOM-IICF and 3DOM-NIICF slowly increased. The increase in the adsorption capacity was due to the increased diffusion of molecules in the solution after an increase in temperature. Because chitosan is unstable at high temperatures, we set the maximum experimental temperature at 323 K. Because $\Delta H > 0$, the adsorption process was endothermic. The spontaneous feasibility of this reaction can also be estimated from the value of ΔG. It can also be seen that 3DOM-IICF has better adsorption performance than 3DOM-NIICF.

3.4.5 Competitive adsorption experiment. To verify the performance of 3DOM-IICF for the selective adsorption of Cu(II), we performed competitive adsorption experiments. The adsorbent selectivity was measured by placing the adsorbent in a solution containing four metal ions (Cu(II), Cr(III), Pb(II) and Zn(II)). The selective adsorption of Cu(II) by 3DOM-IICF was evaluated by K_d, k and k' (distribution coefficient, selectivity

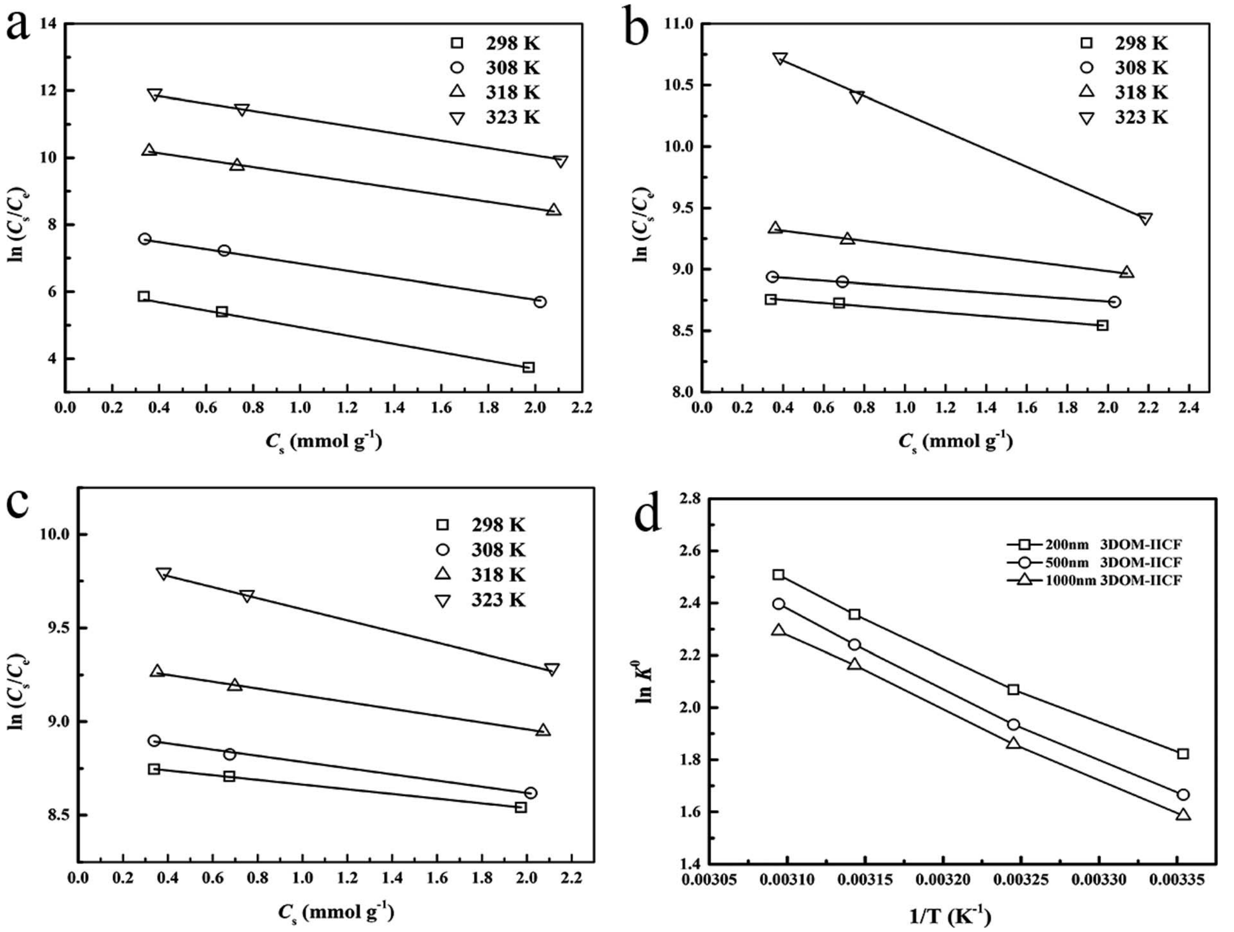

Fig. 10 Thermodynamic properties of Cu(II) at 3DOM-IICF at 298, 308, 318 and 323 K: (a) shows a plot of ln C_s/C_e against C_s of 200 nm; (b) shows a plot of ln C_s/C_e against C_s of 500 nm; (c) shows a plot of ln C_s/C_e against C_s of 1000 nm; (d) shows the van't Hoff plots of ln K^0 against $1/T$.

coefficient and relative selectivity coefficient, respectively). The formulas for K_d, k and k' are as follows:

$$K_d = \frac{C_0 - C_f}{C_f} \times \frac{V}{m} \tag{12}$$

$$k = \frac{k_{d1}}{k_{d2}} \tag{13}$$

$$k' = \frac{k_{\text{3DOM-IICF}}}{k_{\text{3DOM-NIICF}}} \tag{14}$$

where C_0 represents the initial concentration of four ions (50 mg L^{-1}), and C_f represents the final concentration of each ion. Table 4 shows the indices of the other ions (Cr(III), Pb(II) and Zn(II)) relative to those of Cu(II). It can be seen from Fig. 11 that the 3DOM-IICF with three different pore sizes more efficiently adsorbs Cu(II) over other ions, with the most significant being 3DOM-IICF at 500 nm. The relative selectivity coefficient k' represents the affinity of the selective imprinted site of the material to the template ion. It can be seen from Table 5 that the affinities of the 200 nm 3DOM-IICF to other ions are 0.344, 0.336 and 1.022 times that of 3DOM-NIICF; moreover, compared with those of 3DOM-NIICF, the adsorption affinities of 500 nm 3DOM-IICF to Cu(II) are 1.073, 1.190 and 1.390 times that of other ions. Compared with those of the 3DOM-NIICF, the affinities of 3DOM-IICF to Cu(II) at 1000 nm are 0.857, 1.046 and 5.544 times that of other ions.

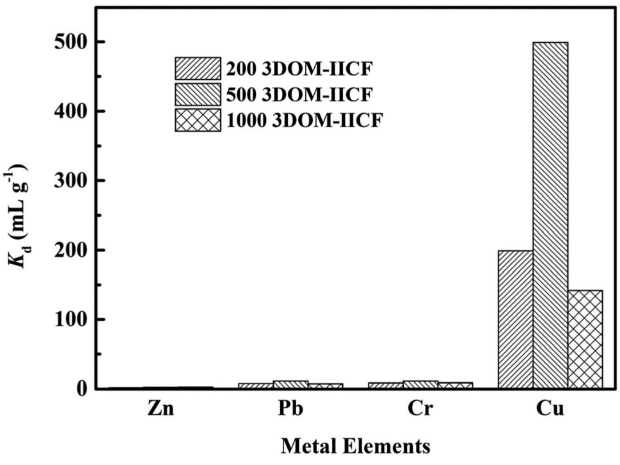

Fig. 11 K_d plot of the 3DOM-IICF obtained *via* the competition experiment.

Table 5 K_d, k and k' values of Cr(III), Pb(II) and Zn(II) with respect to those of Cu(II)

	200 nm 3DOM-IICF			200 nm 3DOM-NIICF			
Metal ions	C_f (mg L^{-1})	K_d (mL g^{-1})	k	C_f (mg L^{-1})	K_d (mL g^{-1})	k	k'
Cu(II)	0.25	199.000		0.24	211.766		
Cr(III)	5.35	8.355	0.042	1.87	25.810	0.122	0.344
Pb(II)	5.69	7.792	0.039	1.95	24.670	0.116	0.336
Zn(II)	16.87	1.964	0.010	16.42	2.045	0.010	1.022
	500 nm 3DOM-IICF			500 nm 3DOM-NIICF			
Metal ions	C_f (mg L^{-1})	K_d (mL g^{-1})	k	C_f (mg L^{-1})	K_d (mL g^{-1})	k	k'
Cu(II)	0.1	499		0.1	499		
Cr(III)	4.22	10.846	0.022	4.50	10.109	0.020	1.073
Pb(II)	4.24	10.79	0.022	4.97	9.066	0.018	1.190
Zn(II)	14.74	2.392	0.005	18.38	1.720	0.003	1.390
	1000 nm 3DOM-IICF			1000 nm 3DOM-NIICF			
Metal ions	C_f (mg L^{-1})	K_d (mL g^{-1})	k	C_f (mg L^{-1})	K_d (mL g^{-1})	k	k'
Cu(II)	0.35	141.857		0.1	499		
Cr(III)	5.13	8.756	0.062	1.35	35.955	0.072	0.857
Pb(II)	5.94	7.412	0.052	1.93	24.920	0.050	1.046
Zn(II)	12.81	2.904	0.020	17.59	1.843	0.004	5.544

Because the imprinted material can elute the template ion, it will leave a space site unique to the template ion inside the material that will be used for the specific adsorption of the template ion. Therefore, in the mixed solution containing various ions, the imprinted film has the best adsorption effect on Cu(II).

The adsorption capacity is the most important factor in evaluating the adsorption performance of an adsorbent. As presented in Table 6, the pH conditions for the adsorption of Cu(II) by TiO_2 and $CaCO_3$ composite chitosan materials are closest to those used in this study. However, their adsorption capacity is far less than that of 3DOM-IICF, and the adsorption capacity achieved herein is 4–7 times that of the TiO_2 and $CaCO_3$ composite chitosan materials. The adsorption capacity of other cross-linked chitosan and chitosan composites is not as high as that of the material proposed herein and is not selective. In general, compared with the materials made by other researchers, our materials not only have strong adsorption capacity, but also good stability, good selective adsorption effect, easy recyclability and reusability. This is due to the excellent 3D ordered porous structure and excellent imprinting technology of the 3DOM-IICF.

3.4.6 Regeneration experiment. Taking into account the prospects of the 3DOM-IICF in industrial applications, we conducted repetitive regeneration experiments. Based on the experimental data, it can be concluded that the material with the 500 nm aperture is most outstanding in the imprinted film. *Via* the repetitive regeneration experiment, the most excellent material for the experiment was selected. The repeatability of Cu(II) is of great importance to the industry. Cu(II) eluted completely with the eluent after each adsorption cycle. Fig. 12 shows the change in the adsorption capacity after each adsorption cycle. Because the imprinted material provides a specific adsorption site for Cu(II), the adsorption efficiency and the possibility of material regeneration are greatly improved. After five cycles, the adsorption performance of the

Table 6 Compared with other chitosan materials

Adsorbents	Ions	Q_m (mg g^{-1})	pH	Selectivity	References
3DOM-IICF	Cu(II)	261.31	7.0	High	This work
Triethylenetetramine modified graphene oxide/chitosan composite	Cr(VI)	219.5	2.0	—	29
Cross-linked chitosan	Cr(VI)	86.81	3.0	—	30
Magnetic amino-thiourea CS–BC composite	Cd(II)	16.97	7.0	—	31
$NTiO_2$-NCh	Cu(II)	63.55	7.0	—	32
Chitosan/$CaCO_3$-silane nanocomposites	Cu(II)	33.9	6.0	—	33

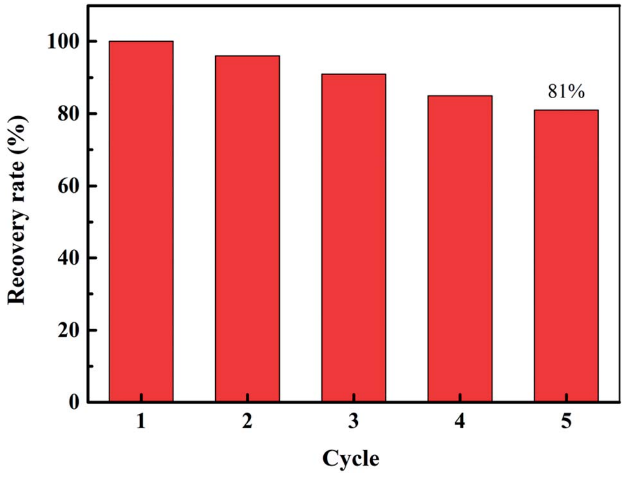

Fig. 12 Regeneration of the 500 nm 3DOM-IICF.

3DOM-IICF decreased by about 19%, and the downward trend tended to be gentle. The possible cause of this phenomenon is the loss of adsorbent material and incomplete elution. The results show that 3DOM-IICF is a feasible and stable adsorbent in practical applications.

4. Conclusion

Herein, high-performance chitosan was prepared by a colloidal crystal template and ion imprinting to adsorb Cu(II) in water. The 3DOM-IICF successfully cross-linked the PS microspheres with three different sizes. *Via* the analysis of morphology, functional groups and thermal stability, it was verified that the structure of the three-dimensional ordered macropores and the thermal stability of the materials after TEOS addition were significantly improved. As 3DOM-IICF has a three-dimensional ordered macroporous structure, the mass transfer efficiency of the adsorption process is improved; this leads to high adsorption efficiency of the material and large adsorption capacity. The 3DOM-IICF can achieve higher adsorption capacity in 5 minutes, and its maximum adsorption capacity is as high as 261.31 mg g^{-1}. Due to the introduction of ion-imprinting technology, the 3DOM-IICF has strong selective adsorption capacity for Cu(II). After five cycles of regeneration, the adsorption capacity still retained as much as 81%. The 3DOM-IICF also has the advantages of strong hydrophilicity, strong structure, good stability, recyclability, *etc.*; therefore, it has great prospects for industrial applications.

Conflicts of interest

There are no conflicts to declare.

Acknowledgements

This work was financially supported by the National Natural Science Foundation of China (No. 21808018, 21876015), Natural Science Research Project of Jiangsu Province (No. 18KJB610002), and Basic Research on the Application of Changzhou (No. CJ20180055).

References

1 T. S. Frantz, N. Silveira Jr, M. S. Quadro, R. Andreazza, A. A. Barcelos, T. R. S. Cadaval Jr and P. Laa, *Environ. Sci. Pollut. Res. Int.*, 2017, **24**, 1–10.
2 C. Xu, *Environ. Sci. Manage.*, 2007, **8**, 020.
3 M. Ahmad, K. Manzoor, P. Venkatachalam and S. Ikram, *Int. J. Biol. Macromol.*, 2016, **92**, 910.
4 X. Wang and C. Wang, *Colloids Surf., A*, 2016, **500**, 186–194.
5 L. Zeng, Y. Chen, Q. Zhang, X. Guo, Y. Peng, H. Xiao, X. Chen and J. Luo, *Carbohydr. Polym.*, 2015, **130**, 333–343.
6 X. Li, H. Zhou, W. Wu, S. Wei, Y. Xu and Y. Kuang, *J. Colloid Interface Sci.*, 2015, **448**, 389.
7 G. Crini, N. Morin-Crini, N. Fatin-Rouge, S. Déon and P. Fievet, *Arabian J. Chem.*, 2014, 71.
8 L. Zhang, Y. Zeng and Z. Cheng, *J. Mol. Liq.*, 2016, **214**, 175–191.
9 J. Deng, Y. Liu, S. Liu, G. Zeng, X. Tan, B. Huang, X. Tang, S. Wang, Q. Hua and Z. Yan, *J. Colloid Interface Sci.*, 2017, **506**, 355–364.
10 F. Zhao, E. Repo, M. Sillanpaa, Y. Meng, D. Yin and W. Z. Tang, *Ind. Eng. Chem. Res.*, 2015, **54**, 1271–1281.
11 M. Aliabadi, M. Irani, J. Ismaeili and S. Najafzadeh, *J. Taiwan Inst. Chem. Eng.*, 2014, **45**, 518–526.
12 E. M. S. Azzam, G. Eshaq, A. M. Rabie, A. A. Bakr, A. A. Abd-Elaal, A. E. E. Metwally and S. M. Tawfik, *Int. J. Biol. Macromol.*, 2016, **89**, 507–517.
13 S. Peng, H. Meng, Y. Ouyang and J. Chang, *Ind. Eng. Chem. Res.*, 2014, **53**, 2106–2113.
14 Z. C. Lv and Q. Li, *Chem. Bioeng.*, 2017, **34**, 44–47.
15 X. L. Zhang, Z. G. Dai, X. G. Zhang, S. L. Dong, W. Wu, S. K. Yang, X. H. Xiao and C. Z. Jiang, *Sci. China: Chem.*, 2016, **59**, 126801.
16 X. Zheng, E. Liu, F. Zhang, J. Dai, Y. Yan and C. Li, *Cellulose*, 2016, 1–12.
17 J. H. Chen, H. Lin, Z. H. Luo, Y. S. He and G. P. Li, *Desalination*, 2011, **277**, 265–273.
18 C. Branger, W. Meouche and A. Margaillan, *React. Funct. Polym.*, 2013, **73**, 859–875.
19 G. Z. Kyzas, P. I. Siafaka, E. G. Pavlidou, K. J. Chrissafis and D. N. Bikiaris, *Chem. Eng. J.*, 2015, **259**, 438–448.
20 S. Zarghami, T. Mohammadi and M. Kazemimoghadam, *J. Dispersion Sci. Technol.*, 2015, **36**, 190–195.
21 E. Salehi, S. S. Madaeni and V. Vatanpour, *J. Membr. Sci.*, 2012, **389**, 334–342.
22 X. Wei, Z. Zhang and Z. Wang, *Microchem. J.*, 2019, **145**, 55–58.
23 X. Wei, M. Yu, C. Li, X. Gong, F. Qin and Z. Wang, *Microchim. Acta*, 2018, **185**, 208.
24 X. Wei, G. Xu, C. Gong, F. Qin, X. Gong and C. Li, *Sens. Actuators, B*, 2018, **255**, 2697–2703.
25 X. Zheng, Y. Zhang, T. Bian, Y. Zhang, F. Zhang and Y. Yan, *Cellulose*, 2019, **26**, 1209–1219.
26 X. Zheng, Y. Zhang, F. Zhang, Z. Li and Y. Yan, *J. Hazard. Mater.*, 2018, **353**, 496–504.

27 X. Zheng, Y. Wang, F. Qiu, Z. Li and Y. Yan, *J. Chem. Eng. Data*, 2019, **64**, 926–933.

28 E. Du, J. Li, S. Zhou, L. Zheng and X. Fan, *Chemosphere*, 2018, **211**, 1007–1017.

29 H. Ge and Z. Ma, *Carbohydr. Polym.*, 2015, **131**, 280–287.

30 Z. Wu, S. Li, J. Wan and W. Yan, *J. Mol. Liq.*, 2012, **170**, 25–29.

31 R. Li, L. Wen, H. Hui, S. Jiang, G. Di, M. Li, Z. Zhang, A. Ali and J. J. Wang, *J. Appl. Polym. Sci.*, 2018, **135**, 46239.

32 M. E. Mahmoud, S. A. A. A. Ali and S. M. T. Elweshahy, *Int. J. Biol. Macromol.*, 2018, **111**, 393–399.

33 S. Mallakpour and E. Khadem, *Int. J. Biol. Macromol.*, 2018, **114**, 149–160.